Available online at www.sciencedirect.com
SCIENCE DIRECT®
Journal of Photochemistry and Photobiology A: Chemistry 172 (2005) 241–249
Journal of Photochemistry and Photobiology A:Chemistry
www.elsevier.com/locate/jphotochem

Dissociative excitation of benzonitrile by ultraviolet multiphoton absorption

Jun-ichi Aoyama, Kiyohiko Tabayashi*, Ko Saito

Department of Chemistry, Graduate School of Science, Hiroshima University, Kagamiyama, Higashi-Hiroshima 739-8526, Japan

Received 4 December 2003; received in revised form 2 November 2004; accepted 29 November 2004
Available online 23 January 2005

Abstract

Dissociative excitation of benzonitrile, C_6H_5CN, for generating excited photofragments, CN(*A*) and CN(*B*), was studied with resonantly enhanced multiphoton excitation at 266 nm. Laser power dependence of CN(*A*–*X*) and CN(*B*–*X*) intensities demonstrated that the CN(*A*,*B*) formation takes place via the two-photon absorption process, $C_6H_5CN + 2h\nu \rightarrow C_6H_5(\tilde{X}) + CN(A,B)$. Vibrational and rotational energy distributions of the nascent CN(*A*,*B*) fragments from photoexcited benzonitrile in the VUV energy region were determined by simulation analysis of dispersed fluorescence spectra. For both CN(*A*) and CN(*B*), the vibrational distributions were found to be of the uninverted type and the rotational distribution in each vibrational state could be approximated by a Boltzmann distribution. The best-fit vibrational distribution of CN(*A*) was determined to be $N_{v'=2}:N_{v'=3}:N_{v'=4}:N_{v'=5}:N_{v'=6} = 1.0:0.45:0.16:0.06:0.03$ and the rotational temperature in each vibrational state was $T_r(v' = 2) = 3500$ K, $T_r(v' = 3) = 3200$ K, $T_r(v' = 4) = 2200$ K, $T_r(v' = 5) = 2000$ K, and $T_r(v' = 6) = 2000$ K, respectively. The vibrational distribution of CN(*B*) was $N_{v'=0}:N_{v'=1}:N_{v'=2} = 1.00:0.43:0.18$ with respective rotational temperatures of $T_r(v' = 0) = 2000$ K, $T_r(v' = 1) = 1300$ K, and $T_r(v' = 2) = 1300$ K. The vibrational and rotational distributions of CN(*A*) were found to be hotter than those predicted by the statistical model with complete energy randomization within the excited molecule. These results indicate that the dissociation to $C_6H_5(\tilde{X}) + CN(A)$ proceeds via the mechanism where both vibrational energy deposition in the photoexcitation and available energy redistribution before the dissociation are limited within the internal modes of skeletal C_6–CN structure. The vibrational distribution of CN(*B*) was significantly hotter than the statistical distribution and can be attributed to a fast decay of the photoexcited Rydberg state via an intermediate state onto a repulsive dissociation surface leading to $C_6H_5(\tilde{X}) + CN(B)$.

Keywords: Dissociative excitation; Benzonitrile; CN($A^2\Pi_i - X^2\Sigma^+$); CN($B^2\Sigma^+ - X^2\Sigma^+$); Internal energy distribution; Dissociation dynamics

1. Introduction

Photodissociative excitation of simple cyano compounds RCN (R = H, X, CN) has been frequently studied in the Vacuum Ultraviolet (VUV) region, since strong fragment emissivities of CN($B^2\Sigma^+ - X^2\Sigma^+$) and CN($A^2\Pi_i - X^2\Sigma^+$) enable one to obtain the important information about dynamics in the dissociative excitation channels and their interactions with other decay channels from the VUV photoexcited states. Synchrotron radiation source with good stability and tunability in the broad VUV region provided fluorescence excitation cross sections [1,2] of these cyanides against the wavelength of exciting light. Using intense VUV lasers at 157.6 and 121.6 nm, vibrational and rotational (V/R) state distributions of the dissociative excitation products CN(*A*,*B*) [3,4] were determined from the dispersed fluorescence and laser-induced fluorescence measurements. Ultraviolet (UV) multiphoton laser excitation technique [5] has also been applied to obtain the state distributions of the fluorescent fragments from the VUV excited states.

Photodissociative excitation studies of moderate sized cyanides [6–9] in the VUV energy region have been rather limited. Previously, we have performed fluorescence measurements for acetyl cyanide, CH_3COCN [6], using resonantly enhanced two-photon excitation by UV light at

* Corresponding author. Tel.: +81 824 24 7406; fax: +81 824 24 0727.
E-mail address: tabayasi@sci.hiroshima-u.ac.jp (K. Tabayashi).

1010-6030/$ – see front matter © 2004 Elsevier B.V. All rights reserved.
doi:10.1016/j.jphotochem.2004.11.019

292.0 nm. Internal energy distributions of nascent CN(*B*) determined were of the uninverted type, but they were found to be obviously hotter than those predicted by a simple statistical theory. The hotter internal energy partitioning for the $CH_3CO(\tilde{X}) + CN(B)$ products is then expected when random energy transfer near the transition state is limited within the skeletal CCOCN vibrational modes. A similar dissociation picture is also proposed for the photolysis of acyl cyanides [10,11] at 193 nm, where non-Rice–Ramsperger–Kassel–Marcus (RRKM) rates of CN(*X*) production have been observed. Here, we have determined the product state distributions for both CN(*A*) and CN(*B*) from the photodissociative excitation of benzonitrile by using UV multiphoton excitation technique and examined the dynamics in the dissociation based on simple theoretical models, where the intramolecular vibrational redistribution (IVR) efficiency within the phenyl group is a matter of our concern.

In the present study, we have performed fluorescence measurements of benzonitrile after resonantly enhanced multiphoton absorption at 266 nm. Here, we have chosen S_1, $^1(\pi,\pi^*)$ for the first photoexcitation state and observed CN(*A–X*) and CN(*B–X*) fluorescence in the visible and UV regions. Laser power dependence of the CN(*A–X*) and CN(*B–X*) intensities showed that two-photon absorption is involved in the CN(*A,B*) formation processes. The V/R energy distributions for both CN(*A*) and CN(*B*) were determined by simulation analysis of the fluorescence spectra. The vibrational energy distribution of CN(*B*) was significantly hotter than that predicted by the statistical model with complete energy randomization within the excited molecule, indicating a prompt dissociation on the highly excited repulsive surface. The V/R distributions of CN(*A*) were also found to be hotter than those predicted by the statistical model. The formation of CN(*A*) can be interpreted as the dissociation where internal energy randomization of the system is mostly limited within the restricted modes along the planar C_6–CN structure.

2. Experimental

Experimental apparatus used in the present study has been described elsewhere [6,12]. Briefly, multiphoton excitation of benzonitrile was performed with 1.7–5 mJ pulses of the fourth harmonic output (266 nm) of a Nd:YAG laser at a repetition rate of 10 Hz. The laser beam was mildly focused with a focal quartz lens (f = 450 mm) and introduced into a light-baffled gas cell through an iris. The gas cell was evacuated with a rotary pump backed by a liquid-nitrogen trap, then the ultimate pressure of the gas cell was less than 0.4 mTorr (1 Torr = 133.3 Pa). Fluorescence from the interaction zone in the gas cell was imaged with two focal lenses on an entrance slit of a 0.5 m monochromator. Dispersed fluorescence was then detected with an optical multi-channel analyzer (OMA) mounted on the monochromator. The dispersed spectra were typically recorded by integrating signals over 3000–12,000 laser shots.

Special precautions were taken for the experimental condition of the fluorescence measurements to obtain reliable internal state distributions of the products CN(*A,B*) from the fluorescence spectra. Lurie and Elsayed [9] determined a quenching rate constant for CN(*B*) by CH_4 of $(1.5 \pm 0.5) \times 10^{-10}$ cm^3 molecule^{-1} s^{-1}, corresponding to a relaxation time of $(p\tau)$ = 207 Torr ns. Quenching rates of CN(*A*) were also reported to be $<1.6 \times 10^{-10}$ cm^3 molecule^{-1} s^{-1} by Ar [13,14] and $<2.4 \times 10^{-10}$ cm^3 molecule^{-1} s^{-1} by C_2N_2 [14], which correspond to >129 and >194 Torr ns, respectively. In order to eliminate a possible contribution of collision-induced relaxation on the fluorescence spectra, the product of the sample pressure and observation time (pt) less than bimolecular relaxation time ($p\tau$) is necessary for the dispersed fluorescence measurements. Here, the CN(*B–X*) fluorescence spectrum was typically recorded at a sample pressure of ∼55 mTorr with a gate width of 200 ns. Since radiative lifetime of CN(*B*), 60–80 ns, actually defines the observation time, then $(pt) = \sim 4$ Torr ns $\ll (p\tau) = \sim 200$ Torr ns clearly shows that collisional relaxation is unimportant for the present CN(*B–X*) measurements. The dispersed CN(*A–X*) fluorescence spectra used for the internal state distribution analysis were measured at a pressure of 12 mTorr with a gate width of 1 μs, although CN(*A*) has a longer radiative lifetime of several microseconds, leading to (pt) = 12 Torr ns for the CN(*A–X*) measurements. Recently, Guo et al. [3] found that rotational energy relaxation of CN(*A*) by HCN was also negligible for N = 7 and 18 levels at the conditions of (pt) = 16 and 13 Torr ns. We believe that the collision-induced relaxation is scarcely involved in the present CN(*A–X*) fluorescence measurements under our experimental condition. It should be noted that the collisional relaxation of photoexcited benzonitrile is also negligible since time scales of the dissociation processes from the VUV states are considered to be in the ps range [15].

In order to obtain some of the molecular constants unavailable for $C_6H_5CN(\tilde{X})$ and $C_6H_5(\tilde{X})$, we also performed ab initio MO calculations using the GAUSSIAN 98 programs [16].

Benzonitrile with a stated purity of 99.9% was purchased from Aldrich Chemical Co. It was degassed by several freeze-pump-thaw cycles prior to use.

3. Results and discussion

3.1. Fluorescence measurements

Fig. 1 shows a typical fluorescence spectrum measured in the 240–530 nm region when benzonitrile was excited by 266 nm laser light. This spectrum was recorded with a low resolution (HWHM = 6.7 nm) at a laser power of 4.5 mJ. From a comparison with dispersed fluorescence spectra by Sakota et al. [17], we assigned a broad and intense fluorescence band around 280 nm to S_1–S_0 transition of benzonitrile. Kobayashi et al. [18] demonstrated that a radia-

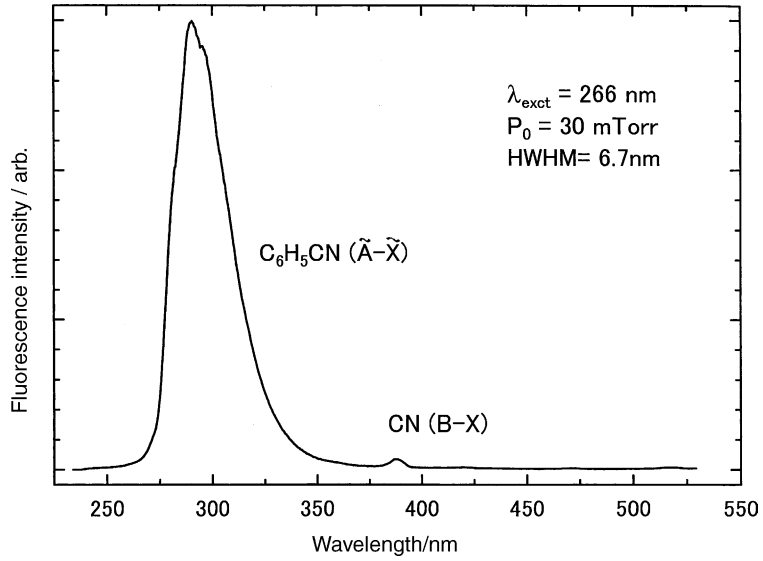

Fig. 1. Fluorescence spectrum in the 240–530 nm region observed from the laser photodissociation of C_6H_5CN at 266 nm. The spectrum was taken at a sample pressure of 30 mTorr with laser pulse energy of 4.5 mJ. Spectral resolution was set at HWHM = 6.7 nm.

tive lifetime of the transition was 42–67 ns in the vibronic region 266.77–273.88 nm. Since the decay time of the S_1 state is longer than the laser pulse duration, resonantly enhanced multiphoton excitation is effective via the S_1 state. By masking the intense S_1–S_0 emission with two long-path filters (HITACHI UV-35), we could observed fluorescence bands in the longer wavelengths. $\Delta v = 0$ sequence of the CN($B^2\Sigma^+ - X^2\Sigma^+$) band system around 390 nm and $\Delta v = 2$, 3, 4 sequences of the CN($A^2\Pi_i - X^2\Sigma^+$) band system in the 600–850 nm region can be ascertained in Fig. 2. No apparent fluorescence bands other than the above were discernible in the spectral range 450–850 nm. The present detection system (OMA) has a limited response in the near IR region to cover the full range of the broad CN($A^2\Pi_i - X^2\Sigma^+$) band system, then a branching ratio for the CN(*A*) and CN(*B*) formation could not be determined. We estimated, however, that the relative CN(*A*) yield lies at a level at least two orders of magnitude larger than the CN(*B*).

In order to examine the dependence of the CN(*A*,*B*) formation on laser photon density, time-integrated fluorescence intensities of the fragments were measured against laser pulse energy. Fig. 3(a) shows a logarithmic plot of the CN(*A*–*X*) intensity and the laser pulse energy at the interaction zone in the gas cell. Linear fit of the data points provided the second or-

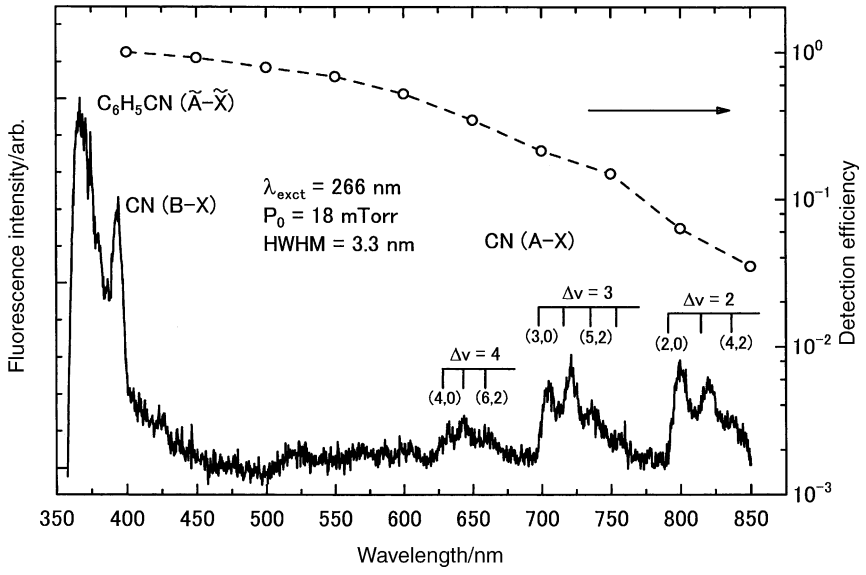

Fig. 2. Fluorescence spectrum in the 360–850 nm region observed from the laser photodissociation of C_6H_5CN at 266 nm. The spectrum was taken at a sample pressure of 18 mTorr with laser pulse energy of 4 mJ. Spectral resolution was set at HWHM = 3.3 nm. Total efficiency of the optical detection system is indicated as a dashed curve.

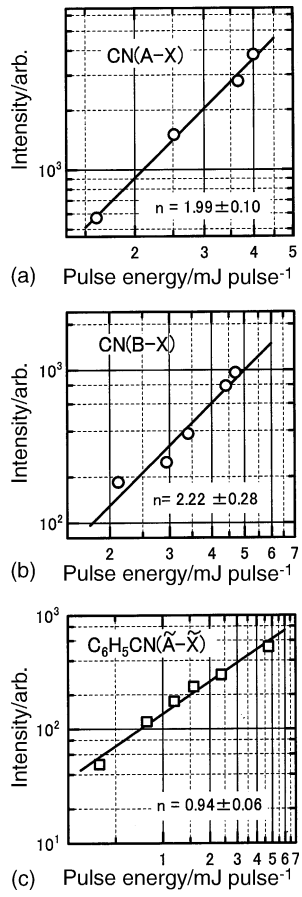

Fig. 3. Logarithmic plots of the fluorescence intensity of the fragment (or photoexcited state) and UV laser power. (a) CN(*A*–*X*), (b) CN(*B*–*X*), (c) $C_6H_5CN(\tilde{A}–\tilde{X})$. The gradient (*n*) of the linear fit to the data points is indicated in each figure.

der behavior on the laser power with a slope $n = 1.99 \pm 0.10$ within the power range 1.7–4 mJ. The same second order behavior of the CN(*B*–*X*) intensity on the laser power was ascertained from the slope ($n = 2.22 \pm 0.28$) of the logarithmic plot (Fig. 3(b)). The first order photon absorption behavior was also checked in Fig. 3(c) by measuring S_1–S_0 fluorescence intensity for the present experimental conditions. A laser power dependence of $n = 0.94 \pm 0.06$ is actually indicative of no saturation in the first photon absorption. It should be also noted that no apparent spectral changes of the CN(*A*–*X*,*B*–*X*) band emission were shown under the present laser conditions. These laser power dependence demonstrate that both CN(*A*) and CN(*B*) formations from benzonitrile take place via a two-photon absorption process at 266 nm.

A dispersed CN(*A*–*X*) fluorescence spectrum recorded with HWHM = 3.3 nm is corrected using an efficiency curve of our optical detection system in Fig. 4, where the CN(*A*–*X*) band is clearly identified from $v' = 2$ to $v' = 6$. In order to analyze the V/R distributions of CN(*A*), we prepared a computer simulation program for the CN($A^2\Pi_i - X^2\Sigma^+$) transition. Rotational line strengths for the CN($A^2\Pi_i - X^2\Sigma^+$) band, in which the $^2\Pi_i$ state lies intermediate between Hund's cases (a) and (b), were calculated using the expressions by Earls [19]. Two spin–orbit components of the CN($A^2\Pi_{1/2,3/2}$) were assumed to be the statistical ratio as expressed in the line strengths. Molecular constants [20] and Franck–Condon factors [21] for the CN($A^2\Pi_i - X^2\Sigma^+$) band were quoted from the literature. Gaussian function was employed as a slit function. As a working hypothesis, it was assumed that the rotational distribution at each vibrational level can be fitted to the Boltzmann defined by an effective rotational temperature. Relative vibrational populations and the rotational temperature at each vibrational state were

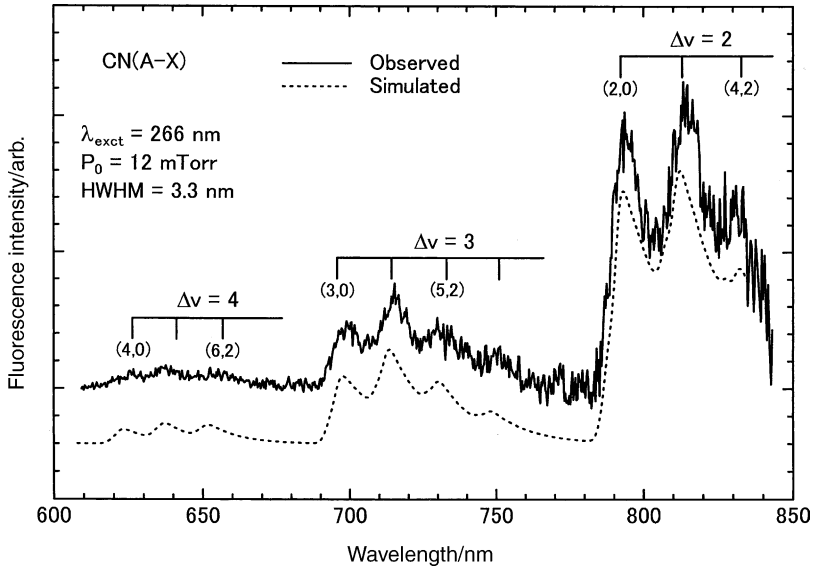

Fig. 4. Comparison of fluorescence spectrum CN(*A*–*X*, $\Delta v = 2, 3, 4$) observed with two-photon excitation at 266 nm with that produced by a computer simulation. The observed spectrum was taken at a sample pressure of 12 mTorr. Spectral resolution was set at HWHM = 3.3 nm. The fluorescence intensity was corrected using the efficiency curve of the optical detection system.

Table 1
Best-fit parameters for CN(*A–X*, $\Delta v = 2, 3, 4$) fluorescence in the two-photon excitation of benzonitrile at 266 nm and populations predicted from the statistical models

Vibrational level	Experimental		Model 1		Model 3	
v'	$N_{v'}/N_2$	$T_r(v')$ (K)	$N_{v'}/N_2$	$T_r(v')$ (K)	$N_{v'}/N_2$	$T_r(v')$ (K)
0	(6.26)		23.7	1720	8.24	2280
1	(2.56)		5.04	1630	2.96	2450
2	1.00	3500 ± 300	1.000	1530	1.000	2280
3	0.45 ± 0.03	3200 ± 300	0.183	1430	0.314	2100
4	0.16 ± 0.02	2200 ± 400	0.0303	1330	0.091	1920
5	0.06 ± 0.02	2000 ± 500	0.0045	1230	0.0239	1750
6	0.03 ± 0.01	2000 ± 500	5.8×10^{-4}	1130	0.0056	1580
7			6.5×10^{-5}	1030	0.0011	1410
f_v	(0.055)		0.021		0.042	

taken as parameters and they were adjusted to give the best-fit of the simulated spectrum to the observed. After the optimal matching between the simulated and observed spectra was achieved, a sensitivity analysis was made by checking the effect of making small change in one parameter while holding the rest constant. The error limit of each parameter was determined to allow the matching of the simulated spectrum to the observed within the noise level of the fluorescence intensity. The optimized simulation results are compared with those observed in Fig. 4. The vibrational distribution of CN(*A*) was thus determined to be $N_{v'=2}:N_{v'=3}:N_{v'=4}:N_{v'=5}:N_{v'=6} = 1.0:0.45 \pm 0.03:0.16 \pm 0.02:0.06 \pm 0.02:0.03 \pm 0.01$, where the relative population is normalized at $v' = 2$. The rotational energy distribution in each vibrational state was generally found to be fitted with a single Boltzmann distribution, providing the temperatures of $T_r(v' = 2) = 3500 \pm 300$ K, $T_r(v' = 3) = 3200 \pm 300$ K, $T_r(v' = 4) = 2200 \pm 400$ K, $T_r(v' = 5) = 2000 \pm 500$ K, and $T_r(v' = 6) = 2000 \pm 500$ K, respectively. The computer modeling results of CN(*A*) distributions are summarized in Table 1. The vibrational population results are plotted in Fig. 5. Since the vibrational populations observed appear to be of the Boltzmann type, the $v' = 0$, 1 values could be estimated by extrapolation. They are also given with parenthesis in Table 1.

Fig. 6 shows a fluorescence spectrum of the CN(*B–X*, $\Delta v = 0$) band observed by two-photon excitation at 266 nm with a resolution of HWHM = 0.19 nm. Vibrational peaks of the CN(*B–X*) can be clearly identified up to $v' = 2$. It can also be seen that the vibrational peak intensity gradually decreases with increasing v'. In order to obtain the

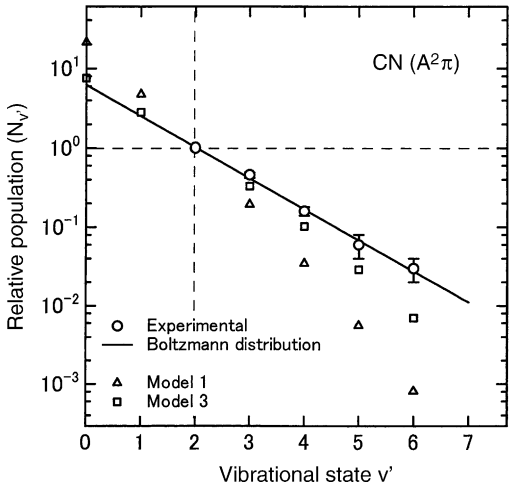

Fig. 5. Semi-logarithmic plots of the CN(*A*,*v*) vibrational distribution. Vibrational population determined by the simulation analysis is compared with those predicted by Model 1 and Model 3. Relative population in each vibrational state is normalized at $v' = 2$.

V/R energy distributions of CN(*B*), population analysis was also carried out using a computer simulation program by Suzuki and Kuchitsu [22]. Simulation parameters were set in a similar manner to the computer modeling of the CN(*A–X*) band. The optimized simulation results of the CN(*B–X*) are also compared with those observed (Fig. 6). The vibrational distribution of CN(*B*) was determined to be $N_{v'=0}:N_{v'=1}:N_{v'=2} = 1.00:0.43 \pm 0.04:0.18 \pm 0.02$. The rotational energy distribution in the each vibrational level was found to be fitted with the temperature of $T_r(v' = 0) = 2000 \pm 400$ K, $T_r(v' = 1) = 1300 \pm 300$ K, and

Table 2
Best-fit parameters for CN(*B–X*, $\Delta v = 0$) fluorescence in the two-photon excitation of benzonitrile at 266 nm and populations predicted from the statistical models

Vibrational level	Experimental		Model 1		Model 2	
v'	$N_{v'}/N_0$	$T_r(v')$/K	$N_{v'}/N_2$	$T_r(v')$ (K)	$N_{v'}/N_0$	$T_r(v')$ (K)
0	1.00	2000 ± 400	1.000	670	1.000	2590
1	0.43 ± 0.04	1300 ± 300	0.0015	290	0.179	1430
2	0.18 ± 0.02	1300 ± 300			0.002	350
f_v	0.214		0.00009		0.068	
f_r		0.221		0.079		0.311

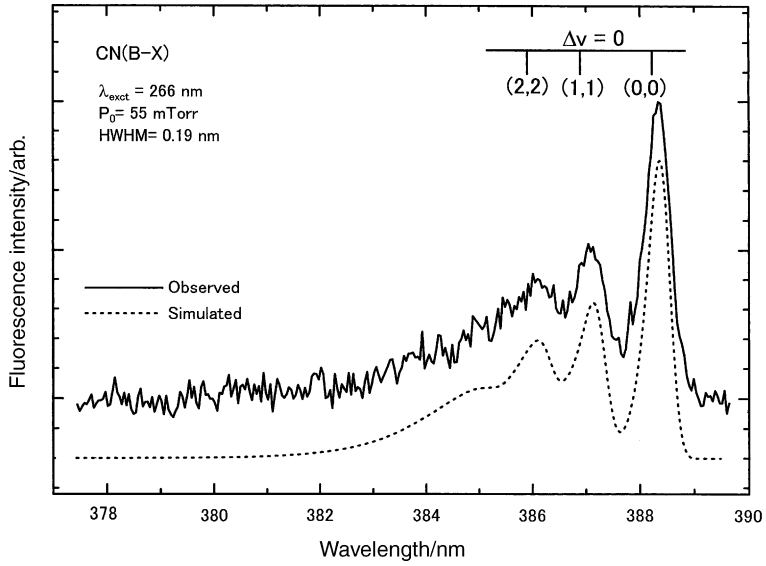

Fig. 6. Comparison of the fluorescence spectrum for CN(*B–X*, $\Delta v = 0$) observed with that produced by a computer simulation. The observed spectrum was taken at a sample pressure of 55 mTorr. Spectral resolution was set at HWHM = 0.19 nm.

$T_r(v' = 2) = 1300 \pm 300$ K, respectively. Best-fit parameters are listed in Table 2.

3.2. Multiphoton dissociation mechanisms for CN(A,B) production

In the above power dependence measurements, the CN(*B*) formation from benzonitrile was shown to take place in the two-photon absorption process at 266 nm. Since one-photon energy at 266 nm (449.7 kJ/mol) is less than the threshold (545 kJ/mol) of dissociation to the ground state pair of $C_6H_5(\tilde{X}) + CN(X)$, the CN(*B*) formation proceeds via a dissociative surface in the vicinity of the direct two-photon excited state,

$$C_6H_5CN \xrightarrow{2h\nu} C_6H_5(\tilde{X}) + CN(B), \quad \Delta H_0^\circ(1) = 854\,\text{kJ/mol} \tag{1}$$

The two-photon laser energy, $E_{ex} = 2 \times 266\,\text{nm} = 899\,\text{kJ/mol}$ (9.32 eV), is close to the ionization threshold of benzonitrile at 9.71 eV (939 kJ/mol) [23], therefore, the initial VUV state accessed in the two-photon excitation step is probably a high-lying Rydberg state. The Rydberg state is actually considered to be short-lived [15], then the dissociation (1) takes place in competition with other fast decay channels.

It is also likely that the photoexcited VUV state decays to the lower electronic states in a cascading manner via internal conversions and/or intersystem crossings. Since the formation threshold of CN(*A*) is much lower than the two-photon excitation energy, the following photodissociative excitation process can be proceed via a lower intermediate electronic state with the same two-photon behavior,

$$C_6H_5CN \xrightarrow{2h\nu} C_6H_5(\tilde{X}) + CN(A), \quad \Delta H_0^\circ(2) = 654\,\text{kJ/mol} \tag{2}$$

In the present dispersed fluorescence spectra of CN(*A–X*), the vibrational transitions from $v' = 2$ to $v' = 6$ were detected (Figs. 2 and 4). If the CN(*A*) fragments were formed via the following dissociation process,

$$C_6H_5CN \xrightarrow{2h\nu} C_6H_5(\tilde{A}) + CN(A), \quad \Delta H_0^\circ(3) = 888\,\text{kJ/mol} \tag{3}$$

Table 3
Photodissociation reactions in the two-photon excitation of benzonitrile at 266 nm

Reaction	ΔH_0° (kJ mol^{-1})	E_{avail} (kJ mol^{-1})
$C_6H_5CN(\tilde{X}) \rightarrow C_6H_5(\tilde{A}) + CN(A)$	888	24
$C_6H_5CN(\tilde{X}) \rightarrow C_6H_5(\tilde{X}) + CN(B)$	854	58
$C_6H_5CN(\tilde{X}) \rightarrow C_6H_5(\tilde{A}) + CN(X)$	779	133
$C_6H_5CN(\tilde{X}) \rightarrow C_6H_5(\tilde{X}) + CN(A)$	654	258
$C_6H_5CN(\tilde{X}) \rightarrow C_6H_5(\tilde{X}) + CN(X)$	545[a]	367

Total excitation energy (912 kJ/mol) includes the two-photon energy E_{ex} and internal energy E_{int} of the parent molecule.

[a] Enthalpy of the reaction, $C_6H_5CN(\tilde{X}) \rightarrow C_6H_5(\tilde{X}) + CN(X)$, was based on $\Delta_f H_{298}^\circ(C_6H_5CN) = 215.7$ kJ/mol [24], $\Delta_f H_{298}^\circ(C_6H_5) = 328.9$ kJ/mol [25], and $\Delta_f H_0^\circ(CN) = 435.4$ kJ/mol [26]. $\Delta_f H_0^\circ(R)$ was calculated from $\Delta_f H_{298}^\circ(R)$ using enthalpy changes of R and reference elements.

they could populate the vibrational states up to $v' = 1$ on the basis of the energetics denoted above. This is not the case for the present CN(*A*–*X*) fluorescence. It is thus concluded that the CN(*A*) products we observed here are only from the process (2). The production pair of $C_6H_5(\tilde{A}) + CN(X)$ is also energetically possible to produce, however, we could not identify any emission other than CN(*A*–*X*,*B*–*X*) in our fluorescence measurements. Table 3 lists the photodissociation channels considered in the two-photon excitation at 266 nm. The energetics are based on several publications of thermochemical and spectroscopic data [24–27].

3.3. Comparison of the V/R distributions of CN(A,B) with statistical calculations

3.3.1. CN(B) formation

The V/R distributions of the products CN(*A*,*B*) can be examined using a statistical prior model [28]. The prior distribution is predicted based on the statistical energy partition between the $C_6H_5(\tilde{X})$ and CN(*A*,*B*) fragments without any angular momentum restriction. In calculating the prior distribution of the V/R levels of CN(*A*,*B*), density of states of polyatomic molecule was approximated by the Whitten–Rabinovitch expression [29]. Rotational density of states was evaluated by that of symmetrical top molecule [30]. Here, the prior distributions were calculated for all the V/R modes of $C_6H_5(\tilde{X}) + CN(A,B)$ (Model 1). The molecular constants [27,31] of the photofragments used for the statistical calculation are listed in Table 4.

In the photodissociation process (1), the available energy to be partitioned into the degrees of freedom of the photofragments is given by

$$E_{\text{avail}} = E_{\text{ex}} - \Delta H_0^\circ(1) + E_{\text{int}} \quad (4)$$

where E_{ex} is the two-photon energy, $E_{\text{ex}} = 2 \times 266\,\text{nm} = 899\,\text{kJ/mol}$, $\Delta H_0^\circ(1) = 854\,\text{kJ/mol}$ is enthalpy change for the process (1) at 0 K, and E_{int} is internal energy of the parent molecule. The internal energy content of benzonitrile at room temperature was calculated to be 13 kJ/mol on the base of molecular constants obtained by ab initio MO calculation [31]. The available energy E_{avail} for the process (1) is 58 kJ/mol. The prior vibrational distribution of CN(*B*) provided $N_{v'=0}:N_{v'=1}:N_{v'=2} = 1.0:0.0015:0.0$. To make an easier comparison with the experimental distribution, the prior rotational distribution in each vibrational level is then characterized [6] using a temperature of the Boltzmann distribution. The present prior results (Model 1) of the V/R distributions of CN(*B*) are listed together with the experimental distributions in Table 2. The fractions of average V/R energy contents to the available energy, $f_v = \langle E_v \rangle / E_{\text{avail}}$ and $f_r = \langle E_r \rangle / E_{\text{avail}}$ are also tabulated for both the experimental and prior distributions.

As described, the prior dissociation Model 1 is defined as the dissociation where statistical energy partitioning into the product degrees of freedom occurs after the complete randomization of the available energy within the excited molecules. The average V/R excitation observed for CN(*B*) were found to be 12.4 and 12.8 kJ/mol which correspond to $f_v = 0.214$ and $f_r = 0.221$, respectively, while the statistical Model 1 predicted the fractional V/R excitation of $f_v(\text{M1}) = 0.00009$ and $f_r(\text{M1}) = 0.079$, respectively. The comparison of these data indicates that the observed distributions are hotter than those predicted by the prior Model 1. In order to examine an efficiency of energy randomization among the internal degrees of freedom, a similar calculation to the prior Model 1 was carried out for the dissociation (Model 2) where all the vibrational modes within the phenyl ring (R) of benzonitrile are set frozen, i.e., R–CN → R + CN(*B*). The calculation led to the vibrational distribution of CN(*B*) of $N_{v'=0}:N_{v'=1}:N_{v'=2} = 1.0:0.179:0.002$ and V/R excitation of $f_v(\text{M2}) = 0.068$ and $f_r(\text{M2}) = 0.311$, respectively (Table 2). The results revealed by the above comparison is that the observed vibrational excitation of CN(*B*) shows a significantly larger population than any "prior" calculation would predict and is not singly due to an inefficiency of the energy randomization, although the rotational degrees of freedom can be available in the Model 2. Following the argument described in Section 3.2, the initially photoexcited Rydberg state can be assumed to decay to the dissociative intermediate state mixed with repulsive Ph–CN natures. The present CN(*B*) formation probably takes place competitively with other ultra fast decay channels onto the repulsive valence surface leading to $C_6H_5(\tilde{X}) + CN(B)$ and there are exit channel effects to give significantly high vibrational excitation of CN(*B*) in the course of dissociation. The significant amount of energy ap-

Table 4
Vibrational frequencies and rotational constants of $C_6H_5(\tilde{X})$ and CN(*A*,*B*) photofragments used for the statistical calculations

Product	Vibrational frequency[c] (cm^{-1})	Rotational constant (cm^{-1})
$C_6H_5(\tilde{X})$[a]	386, 411, 578, 595, 646, 693, 783, 854, 918, 947,	0.2092
	949, 985, 1019, 1041, 1140, 1141, 1268, 1292,	0.1868
	1421, 1433, 1534, 1585, 3059, 3065, 3078, 3080, 3089	0.09870
CN(*A*)[b]	1787.3	1.7066
CN(*B*)[b]	2123.5	1.9615

[a] Vibrational frequencies and rotational constants of $C_6H_5(\tilde{X})$ were obtained here from ab initio MO calculation at the UB3LYP/6-31G(*d*) level of theory. The frequencies are scaled using a factor of 0.9613.
[b] Reference [27].
[c] Underlined frequency is that of skeletal vibration for C_6-ring structure.

pearing in the CN(*B*) vibration is thus understood as the result of a prompt dissociation along the strongly repulsive Ph–CN coordinate. Here, a severe rotational excitation of the CN(*B*) product is not expected in the final state interaction unless a bent type intermediate is involved in the photoexcitation and decay steps. The fitting of the Boltzmann distribution over the rotational levels may be indicative of a possible barrier on to the exit repulsive surface.

3.3.2. CN(A) formation

The CN(*A*) photofragment is formed via the dissociation process (2) with available energy of E_{avail} = 258 kJ/mol upon two-photon excitation at 266 nm (Table 3). In order to investigate the mechanism of the dissociation to $C_6H_5(\tilde{X})$ + CN(*A*), the prior calculation was also performed based on the Model 1 in a similar manner to the case of CN(*B*) formation. The prior vibrational distribution of CN(*A*) provided $N_{v'=2}$:$N_{v'=3}$:$N_{v'=4}$:$N_{v'=5}$:$N_{v'=6}$:$N_{v'=7}$ = 1.0:0.183:0.0303:0.0045:5.8E−04:6.5E−05. The prior results (Model 1) of the V/R distributions for CN(*A*) are listed together with the experimental distributions in Table 1. The average vibrational excitation observed for CN(*A*) could be estimated at 14.2 kJ/mol which corresponds to f_v = 0.055, while Model 1 predicted the fractional vibrational excitation of f_v(M1) = 0.021. A higher rotational temperature than the predicted by Model 1 is also observed in each vibrational state (Table 1). These comparisons show that the observed V/R distributions are obviously hotter than those by Model 1.

In the previous dissociative excitation studies [6], we reported that the two-photon excitation of CH_3COCN at 292 nm produced hotter CN(*B*) photofragments than those predicted by the statistical model with complete energy randomization within the excited molecule. The dissociation was explained as a consequence that the energy randomization takes place among the limited internal modes (the skeletal modes of CH_3COCN) since the CN(*B*) formation process is competitive with other fast decay processes. In the present study, another prior calculation similar to the previous model was carried out to check the efficiency of internal energy randomization within the parent molecule. Model 3 employed here is the dissociation where the internal energy transfer is limited within the skeletal structure of C_6H_5CN, i.e., C_6–CN → C_6 + CN(*A*) (C_6 denotes simple carbon ring structure). The calculation leads to a vibrational distribution of CN(*A*) of $N_{v'=2}$:$N_{v'=3}$:$N_{v'=4}$:$N_{v'=5}$:$N_{v'=6}$:$N_{v'=7}$ = 1.0:0.331:0.102:0.0287:00073:0.0016 and fractional vibrational excitation of f_v = 0.043 (Table 1). The vibrational distributions predicted by Models 1 and 3 are also plotted in Fig. 5 to compare with the observed vibrational distribution. The result by Model 3 is located closer to the observed than that by Model 1, and a similar comparison can be made for the rotational temperatures of the CN(*A*) states (Table 1). These findings clearly indicate incomplete energy randomization among the internal degree of freedom before the bond dissociation occurs. The Model 3 suggests not all (12) of the vibrational modes for the C_6-ring structure but a limited number of its vibrational modes may contribute to the random energy transfer near the transition state.

The present non-statistical behavior of the CN(*A*) products is probably due to the limited internal energy deposition during the optical excitation and slow vibrational energy redistribution in the subsequent internal conversions to the dissociation surface. The excited state, S_1 accessed by the first photon absorption of benzonitrile has been assigned to (π–π^*) transition [17,32], and the structure of the S_1 was characterized on the basis of the correlation [33,34] with excited states of benzene. As described earlier, the two-photon resonance excitation probably produces a high-lying Rydberg state, which is one of the $(\pi_2/\pi_3)^{-1}$ Rydberg members [35] converging to the first or second ionization limits, $C_6H_5CN^+$ ($\tilde{X}^2B_1/\tilde{A}^2A_2$) at 9.71/10.17 eV. Since the first and second photoexcited states thus involve the transitions of the π/π^* electrons with delocalized characters in the C_6 structure, some of the geometrical change in the planar C_6 and CN conjugated moiety may take place prior to the dissociation. In the photoelectron studies [23], for example, the first ionization band of benzonitrile was reported to have vibrational progressions of ∼1128 and ∼488 cm^{-1} corresponding to the skeletal modes of the phenyl ring. Accordingly, vibrational energy is more or less deposited along the C_6–CN modes upon Franck–Condon excitations to the two-photon excited state and then the system undergoes the fast internal conversion down to the lower electronic state where the dissociative excitation of $C_6H_5(\tilde{X})$ + CN(*A*) takes place. The IVR rate is probably slower than that of internal conversion, then the vibrational excitation may be relayed to the lower states along the same C_6–CN coordinates. Since dissociative state to form $C_6H_5(\tilde{X})$ + CN(*A*) is again competitive with other decay channels, complete energy randomization within the entire phase space cannot be expected before the bond dissociation occurs. The uninverted type features of the V/R distributions observed in the CN(*A*) formation, however, indicate that the time on the dissociation surface is long enough for the system to redistribute its excess energy within the restricted vibrational modes along the planar C_6–CN moiety.

4. Conclusion

Dissociative excitation of benzonitrile to produce CN(*A*) and CN(*B*) fragments has been studied by resonantly enhanced multiphoton absorption at 266 nm. Dispersed fluorescence spectra from CN(*A*,*B*) generated via two-photon direct absorption process were analyzed to determine the vibrational and rotational distributions of nascent CN(*A*,*B*) products by computer simulation procedures. Internal energy distributions for both CN(*A*) and CN(*B*) are found to be of the uninverted type, but they are actually hotter than those predicted by a simple statistical theory. Significant vibrational excitation observed in the CN(*B*) products suggests that the

two-photon excited Rydberg state undergoes ultrafast decay to intermediate state which subsequently dissociates on the repulsive $C_6H_5(\tilde{X}) + CN(B)$ surface. We also proposed that the non-statistical behavior of the CN(A) states produced via a lower intermediate electronic state is due to the localized internal energy distribution and slow IVR prior to the dissociation. The observed hotter internal energy partitioning than the statistical for the $C_6H_5(\tilde{X}) + CN(A)$ dissociation is then expected when random energy sampling near the transition state is limited within the restricted C_6–CN vibrational modes due to the competition with fast decay channels.

Acknowledgement

The authors thank the Computer Center of the Institute for Molecular Science for allocation of Fujitsu VPP5000 computer time.

References

[1] For review K. Shobatake, A. Hiraya, K. Tabayashi, T. Ibuki, , in: C.Y. Ng (Ed.), Vacuum Ultraviolet Photoionization and Photodissociation of Molecules and Clusters, World Scientific, Singapore, 1991, pp. 503–562.
[2] (a) For example K. Kanda, M. Kono, T. Nagata, A. Hiraya, K. Tabayashi, K. Shobatake, Chem. Phys. 255 (2000) 369;
(b) K. Kanda, S. Katsumata, T. Nagata, T. Kondow, A. Hiraya, K. Tabayashi, K. Shobatake, Chem. Phys. 218 (1997) 199.
[3] J. Guo, R. Eng, T. Carrington, S.V. Filseth, J. Chem. Phys. 112 (2000) 8904.
[4] (a) For example R. Eng, H.M. Lambert, R. Fei, T. Carrington, S.V. Filseth, Chem. Phys. Lett. 261 (1996) 651;
(b) G.P. Morley, I.R. Lambert, M.N. Ashfold, K.N. Rosser, C.M. Western, J. Chem. Phys. 97 (1992) 3157;
(c) J.A. Guest, F. Webster, J. Chem. Phys. 86 (1987) 5479.
[5] (a) For example B.B. Craig, W.L. Faust, J. Phys. Chem. 87 (1983) 4568;
(b) R.J. Donovan, C. Fotakis, A. Hopkirk, C.B. McKendrick, A. Torre, Can. J. Chem. 61 (1983) 1023.
[6] J. Aoyama, T. Sugihara, K. Tabayashi, K. Saito, J. Chem. Phys. 118 (2003) 6348.
[7] M. Moriyama, Y. Tsutsui, K. Honma, J. Chem. Phys. 108 (1998) 6215.
[8] S. Uchida, K. Tabayashi, M. Tanaka, O. Takahashi, K. Saito, M. Kono, T. Ibuki, Chem. Phys. Lett. 282 (1998) 375.
[9] J.B. Lurie, M.A. El-sayed, Chem. Phys. Lett. 70 (1980) 251.
[10] I.-R. Lee, W.-K. Chen, Y.-C. Chung, P.-Y. Cheng, J. Phys. Chem. 104 (2000) 10595.
[11] I.-R. Lee, Y.-C. Chung, W.-K. Chen, X.-P. Hong, P.-Y. Cheng, J. Chem. Phys. 115 (2001) 10656.
[12] K. Tabayashi, J. Aoyama, M. Matsui, T. Hino, K. Saito, J. Chem. Phys. 110 (1999) 9547.
[13] D.H. Katayama, T.A. Miller, V.E. Bondybey, J. Chem. Phys. 71 (1979) 1662.
[14] M.R. Taherian, T.G. Slanger, J. Chem. Phys. 81 (1984) 3814.
[15] X.-P. Hong, W.-K. Chen, P.-Y. Cheng, Chem. Phys. Lett. 350 (2001) 495.
[16] M.J. Frisch, G.W. Trucks, H.B. Schlegel, et al., Gaussian'98, Revision A9, Gaussian Inc, Pittsburgh, PA, 1998.
[17] K. Sakota, K. Nishi, K. Ohashi, H. Sekiya, Chem. Phys. Lett. 322 (2000) 407.
[18] T. Kobayashi, K. Homma, O. Kajimoto, S. Tsuchiya, J. Chem. Phys. 86 (1987) 1111.
[19] L.T. Earls, Phys. Rev. 48 (1935) 423.
[20] A.J. Kotlar, R.W. Field, J.I. Steinfeld, J.A. Coxon, J. Mol. Spectrosc. 80 (1980) 86.
[21] R.J. Spindler, J. Quant. Spectrosc. Radiat. Transf. 5 (1965) 165.
[22] K. Suzuki, K. Kuchitsu, Bull. Chem. Soc. Jpn. 50 (1977) 1449.
[23] J.W. Rabalais, R.J. Colton, J. Electron. Spectrosc. Relat. Phenom. 1 (1972/73) 83.
[24] J.B. Pedley, R.D. Naylor, S.P. Kirby, Thermochemical Data of Organic Compounds, 2nd ed., Chapman, New York, 1986.
[25] D.F. McMillen, D.M. Golden, Ann. Rev. Phys. Chem. 33 (1982) 493.
[26] Y. Yuang, S.A. Barts, J.B. Halpern, J. Phys. Chem. 96 (1992) 425.
[27] K.P. Huber, G. Herzberg, Molecular Spectra and Molecular Structure IV, Van Nostrand–Reinhold, New York, 1979.
[28] (a) J.I. Steinfeld, J.S. Francisco, W.L. Hase, Chemical Kinetics and Dynamics, 2nd ed., Prentice-Hall, New Jersey, 1998;
(b) T. Baer, W.L. Hase, Unimolecular Reaction Dynamics, Oxford University Press, Oxford, 1996.
[29] D.C. Tardy, B.S. Rabinovitch, G.Z. Whitten, J. Chem. Phys. 48 (1968) 1427.
[30] K.A. Holbrook, M.J. Pilling, S.H. Robertson, Unimolecular Reactions, 2nd ed., Wiley, New York, 1996.
[31] Molecular constants of C_6H_5CN in the ground state were calculated at the B3LYP/6-31G(d) level of theory.
[32] R.M. Helm, H.-P. Vogel, H.J. Neusser, Chem. Phys. Lett. 270 (1997) 285.
[33] L. Chia, L. Goodman, J.G. Philis, J. Chem. Phys. 79 (1983) 593.
[34] J.H.S. Green, D.J. Harrison, Spectrochim. Acta A 32 (1976) 1279.
[35] K. Kimura, S. Katsumata, Y. Achiba, et al., Handbook of HeI Photoelectron Spectra of Fundamental Organic Molecules, Japan Scientific Society, 1981.